Nanoporous Quantum Filters: Inside Vapor−Liquid Transitions of Quantum Fluids in Nanopores

Piotr Kowalczyk,*,† Piotr A. Gauden,‡ and Artur P. Terzyk‡

Applied Physics, RMIT University, GPO Box 2476 V, Victoria 3001, Australia, and Department of Chemistry, Physicochemistry of Carbon Materials Research Group, N. Copernicus University, Gagarin St. 7, 87-100 Torun, Poland

Received: November 24, 2009; Revised Manuscript Received: February 28, 2010

We study the impact of quantum fluctuations on the phase diagram of a realistic quantum liquid, namely, neon confined in atomistic carbon nanopores at 35 K. Due to the action of attractive solid−fluid potential, both classical and quantum neon vapor condense at lower pressures in carbonaceous nanopores than bulk neon. However, we found that continuous van der Waals s-shaped isotherms, which include stable, metastable, and unstable states computed from classical simulations, are shifted to lower values of pressures in comparison to those from path integral calculations. This systematic underestimation of equilibrium vapor−liquid transition pressures as well as spinodals in classical simulations is caused by neglecting the zero-point motion of adsorbed neon at 35 K. Delocalized neon atoms excluded more volume in the adsorbed phase than the classical neon particles. Thus, adsorbed and compressed liquidlike phases of quantum neon in the studied nanopores are characterized by lower densities than their classical counterparts. Interestingly, equilibrium vapor−liquid transition pressures of confined neon at 35 K computed from classical simulations are shifted to lower values in comparison to those computed from quantum simulations by ≈30% for different pore sizes. Simulations of classical neon at higher effective temperatures reveal that liquidlike phases of confined quantum neon at 35 K look like classical ones at higher effective temperature of 37 K. Our calculations clearly show that quantum fluctuations cannot be neglected in calculations of phase transitions of quantum fluids at cryogenic temperatures.

I. Introduction

There are thousands of new nanomaterials produced every year. However, only some of them are promising *cryogenic quantum filters*, i.e., nanoporous materials being able to separate quantum mixture components via equilibrium condensation mechanism at cryogenic temperatures.[1,2] Experimental investigations of adsorption, wetting, compression, and condensation of quantum fluids in all produced nanomaterials are impractical due to the high cost of time-consuming cryogenic measurements. Moreover, the difficulty in preparing homogeneous, well-defined, pure and reproducible samples can be responsible for high experimental errors connected with low temperature adsorption measurements. Even for an ideal crystal of a nanomaterial, precise determination of thermodynamic quantities near vapor−liquid phase transition at cryogenic temperatures is real state-of-the-art because of singularities.[3] As a guide for development of optimized nanostructures, computer simulations offer an alternative tool for the investigation of the structure of quantum fluids confined in novel nanoporous membranes and storage vessels.[4−20] When the underlying physical conditions and the intermolecular potentials are known, computer simulations are a convenient vehicle for exploring experimental results for conditions difficult to access experimentally, such as the investigated measurements near the phase transitions at cryogenic temperatures.

The separation of quantum particles at cryogenic temperatures is based on the simple phenomenon, i.e., the first-order vapor−liquid phase transition. The condensation pressure of the confined quantum fluid strongly depends on its interactions with host nanomaterial and zero-point motion.[20−25] The effect of the solid−fluid interaction potential can be tuned by adjusting a size and topology of nanopores.[20,21] Quantum fluctuations of light particles depend on their mass and operating conditions. Let us consider a simple example, namely a mixture of neon and helium. High purity noble gases, including neon, helium, argon, and xenon, are very important for lasers, light bulbs, scuba diving lights, etc.[1] Thus, the separation of noble gases is interesting for both experimentalists and theoreticians. For the same crystal of nanomaterial, neon gas condenses at lower pressures in nanopores than helium because of stronger dispersion energy with the host nanomaterial, and lower zero-point motion. As a result, a fluid mixture in nanopores is enriched in the neon liquidlike phase, since the condensed and compressed neon blocks the nanospaces for helium. *Clearly, the efficiency of this cryogenic separation via equilibrium condensation mechanism strongly depends on the difference between the condensation pressures of quantum mixture components*. The wider is the gap between the vapor−liquid condensation pressures of the mixture components, the higher the efficiency of the quantum mixture separation is.

For a fixed temperature, the separation efficiency can be tuned by the size and topology of nanopores.[20−25] Note that in the nanoscale a small variation in a size and topology of the host material nanopores can significantly increase or decrease the separation efficiency.[20,21] That is why computer simulations are a cheap and convenient tool for tailoring nanopores to optimize

* Corresponding author. Tel: +61 (03) 99252571. Fax: +61 (03) 99255290. E-mail: piotr.kowalczyk@rmit.edu.au.
† RMIT University.
‡ N. Copernicus University.

10.1021/jp911189j
Published on Web 03/26/2010

the efficiency of cryogenic separation.[25] However, one should bear in mind that at low temperatures the quantum fluctuations of light molecules cannot be neglected.[26] Thus, any computational modeling of realistic quantum fluids adsorbed and compressed in nanopores of the host material should take into account the quantum nature of their interactions. Finally, we point out that the standard simulation in the grand canonical ensemble cannot be directly used for prediction of phase transitions in nanopores. The grand canonical Monte Carlo simulation inevitably suffers from difficulty in determining the thermodynamic equilibrium pressure because of pronounced adsorption−desorption hysteresis, which may in some case be an artifact.[27−32] The adsorption and desorption branch of the hysteresis loop are "out-of-equilibrium transitions".[27−32]

In the current paper we study the impact of the quantum fluctuations on the first-order vapor−liquid phase transition of neon adsorbed in atomistic slit-shaped carbon pores at 35 K. Neon is a prototype of the quantum fluid. As does helium, neon disobeys the law of corresponding states.[33,34] However, its zero-point motion is lower than in helium. In the current work we want to answer the following questions: How do quantum fluctuations modify the phase diagram of confined neon? Can we reproduce the entire phase diagram of confined quantum neon at 35 K by its classical counterpart at a higher effective temperature? Is the effective temperature close to the measuring one? In section II, we describe all computation details including molecular models, simulation procedures, and definition of thermodynamic quantities used in the current study. Next, we present a discussion of simulation results. We concentrate our discussion on the impact of quantum fluctuations on the phase diagram of confined neon.

II. Computational Details

II.1. Molecular Models (Path Integral Action). We studied the static and thermodynamic properties of neon adsorbed and compressed in atomistic slit-shaped carbon nanopores at 35 K using two simulation techniques, e.g., grand canonical path integral Monte Carlo simulation (GCPIMC), and gauge cell path integral Monte Carlo simulation (GPIMC).[35−38] According to Feynman's path integral formalism we mapped each neon atom onto an equivalent polymer chain or "necklace" of P classical "beads" $\mathbf{r}_i^{(1)}$, $\mathbf{r}_i^{(2)}$, ..., $\mathbf{r}_i^{(P)}$. The vector $\mathbf{r}$ denotes the position of a bead belonging to the ith atom. In our simulations we have used the primitive action, given by[39−44]

$$W = \frac{mP}{2\beta^2\hbar^2}\sum_{i=1}^{N}\sum_{\alpha=1}^{P}(\mathbf{r}_i^{(\alpha)} - \mathbf{r}_i^{(\alpha+1)})^2 + \frac{1}{P}\sum_{i<j}\sum_{\alpha=1}^{P}V_{ff}(\mathbf{r}_{ij}^{(\alpha)}) + \frac{1}{P}\sum_{i=1}^{N}\sum_{\alpha=1}^{P}V_{sf}(\mathbf{r}_i^{(\alpha)}) \quad (1)$$

where N is the number of neon atoms, $\beta = (k_B T)^{-1}$ is the inverse of the temperature, m denotes the mass of quantum particle, and $\hbar$ is Planck's constant divided by 2π. Owing to the cyclic condition of the polymer chains, if $\alpha = P$, then $\alpha + 1 = 1$. The first two terms in the primitive action given by eq 1 correspond to neon−neon interactions, and the last term results from additional neon−carbon interactions. The interaction potential between neon atoms, $V_{ff}(r)$, is HFD-B, taken from Aziz and Slaman.[45] The interaction potential between neon and carbon atoms, $V_{sf}(r)$, is expressed by the (12,6) Lennard-Jones potential. We note that the Bose statistics has to be attached in PIMC calculations when the degeneracy temperature, T_D, is close to the studied one. Following Ceperley,[41,42] the degeneracy temperature can be estimated from the relation $T_D = \rho^{2/3}\hbar^2/mk_B$, where ρ denotes density of the quantum fluid. At the highest studied density of confined neon of 59 mmol cm^{-3}, $T_D = 0.26$ K, which is far below the investigated temperature. Moreover, for 35 K, the de Broglie wavelength corresponding to the neon atom, $\lambda = 0.656$ Å, is far below its collision diameter, 2.789 Å. We are thus confident that the Bose exchange effects will not have any effect on our results within the numerical accuracy and thus can be neglected in our PIMC simulations. In all simulations at 35 K we quantized the neon atom by a cyclic polymer consisting of 64 beads. We used Lorentz−Berthelot mixing rules to extract Lennard-Jones parameters for neon−carbon interactions:[46,47]

$$\sigma_{Ne-C} = (\sigma_{Ne} + \sigma_C)/2 \qquad \varepsilon_{Ne-C}/k_B = \sqrt{(\varepsilon_{Ne}/k_B)(\varepsilon_C/k_B)} \quad (2)$$

For carbon and neon, we adapted the following values of parameters: $\sigma_C = 3.4$ Å, $\varepsilon_C/k_B = 28$ K, $\sigma_{Ne} = 2.789$ Å, $\varepsilon_{Ne}/k_B = 36.814$ K.[48,49]

II.2. Grand Canonical Path Integral Monte Carlo Method. Gibbs excess isotherms of classical and quantum neon adsorbed in atomistic slit-shaped carbon nanopores at 35 K were calculated by using grand canonical path integral MC simulations. In all performed simulations, the walls of nanopores were modeled by infinite atomistic single-graphitic planes. The chemical potential computed in the canonical ensemble was an input in the grand canonical MC simulations. The relation between density and the chemical potential of neon computed in the canonical ensemble was used for the calculation of the activity of neon in grand canonical MC simulations (for details see our previous works[6,50]). Our simulation systems consist of a cubic simulation box of size $10\sigma_{Ne} \times 10\sigma_{Ne} \times H$, where H denotes the geometric size of the slit-shaped pore (i.e., the distance between the plane passing through all carbon atom centers of the outermost layer of the one wall and the corresponding plane of the opposite wall). During all performed classical and quantum simulations, the graphitic planes were kept rigid. We used periodic boundary conditions in x and y directions with minimum image convention for calculation of molecular interactions.[46,47] As in our previous studies, fluid−fluid interactions between the adsorbed molecules were cut at $r_{cut} = 5\sigma_{Ne}$.[6,50] Thermalization of the adsorbed neon is performed by path-displacement trials (i.e., centroid displacement and bisection[41,42]) whereas chemical equilibration between adsorbed neon and the reservoir is realized by the path exchange trials. The acceptance probabilities are given by the Metropolis algorithm.[46,47] In all classical and quantum grand canonical MC simulations 10^8 configurations were used, of which we discarded the first 6×10^7 to guarantee equilibration. The stability of the simulation results was confirmed by additional longer runs of 5×10^8 configurations. All computed thermodynamic properties of adsorbed neon were fully reproducible.

II.3. Gauge Cell Path Integral Monte Carlo Method. In the current work we extended the gauge cell MC algorithm due to Neimark and Vishnyakov[38,51−54] to simulation of quantum particles in the external field. Similar to classical gauge cell MC, the simulation system consists of two cells: gauge and pore. The length of the pore cell is equal to $10\sigma_{Ne}$. Due to the slit shape of the pore cell, the periodic boundary conditions were applied in the direction parallel to the pore wall.[6,50] As a gauge cell, we employed a cube with triply periodic boundary

conditions. The size of the gauge cell varied from $30\sigma_{Ne}$ to $120\sigma_{Ne}$ and was adjusted so that the sufficient number of cyclic paths (>30) were contained in the gauge cell during the simulation.[38] The gauge cell was calibrated by a series of path integral MC simulations in canonical ensemble with Widom's particle insertion method.[55] Two types of Monte Carlo moves are performed: path displacement within the cells and path exchange between the cells.[38] In the displacement step the cells are independent and represent two unrelated canonical ensembles. The displacement step consists of two steps. First, the whole selected cyclic path is moved according to the displacement of the centroid.[41,42] Next, the selected cyclic path was displaced according to the "bisection" method.[41,42] The displacement step size has been adjusted to give an acceptance ratio of 50%. The exchange step consists of an attempted cyclic path insertion in one of the cells coupled with attempted cyclic path deletion in the other cell. The position for the attempted cyclic path insertion and the cyclic path for the attempted deletion are chosen at random. The acceptance probabilities for both cyclic path displacement and exchange are given by the Metropolis algorithm.[35,36] Each move (displacement in both pore and gauge cell, exchange cyclic path from pore to gauge cell, and in the reverse direction) has the same probability of occurrence. Such selection guarantees the microscopic reversibility since for the exchange trial from pore to gauge cell and in the reverse direction, the probability was equal. Obviously, in the limit $P = 1$ (i.e., in the classical limit) the path integral gauge cell MC is reduced to the standard gauge cell MC due to Neimark and Vishnyakov.[38] In all classical and quantum gauge cell MC simulations 10^8 configurations were used, of which we discarded the first 6×10^7 to guarantee equilibration. The stability of the simulation results was confirmed by additional longer runs of 5×10^8 configurations. All computed thermodynamic properties of adsorbed neon were fully reproducible.

II.4. Gibbs Excess of Adsorption. The Gibbs excess value of adsorption is computed from the following equation:[51−54]

$$\Gamma_{exc} = \langle N \rangle - \rho_b V \tag{3}$$

Here ρ_b denotes the bulk density of neon computed in canonical ensemble, $\langle N \rangle$ is the ensemble average of the number of neon atoms in the simulation box of volume, $V = 10\sigma_{Ne} \times 10\sigma_{Ne} \times H_{eff}$, $H_{eff} = H - \sigma_C$. For investigated operating conditions, Gibbs excess value of adsorption is equal to absolute value of adsorption since for both classical and quantum neon $\langle N \rangle \gg \rho_b V$.

II.5. Vapor−Liquid Phase Transitions in Nanopores. To determine the equilibrium pressure corresponding to coexistence of vapor and liquid classical/quantum neon in fixed slit-shaped carbon pore size, we computed the grand potential by thermodynamic integration along the continuous isotherm starting from a reference ideal gas state at sufficiently low vapor pressure, $\Omega(\mu_r,T) = -k_B T N_r$:[51−54]

$$\Omega(\mu,T) = \Omega(\mu_r,T) - \int_{\mu_r}^{\mu} N(\mu',T)\, d\mu' \tag{4}$$

where $N(\mu)$ denotes the grand canonical ensemble average number of neon atoms corresponding to the fixed chemical potential μ. Note that the full phase diagram of confined classical and quantum neon in the form of the s-shaped van der Waals isotherm, which includes stable, metastable, and unstable states allow precise determination of equilibrium first-order vapor−liquid phase transition as well as vaporlike and liquidlike spinodals. Direct observation of metastable and unstable states of confined neon at atomistic level is an advantage of gauge cell over grand canonical path integral MC technique.

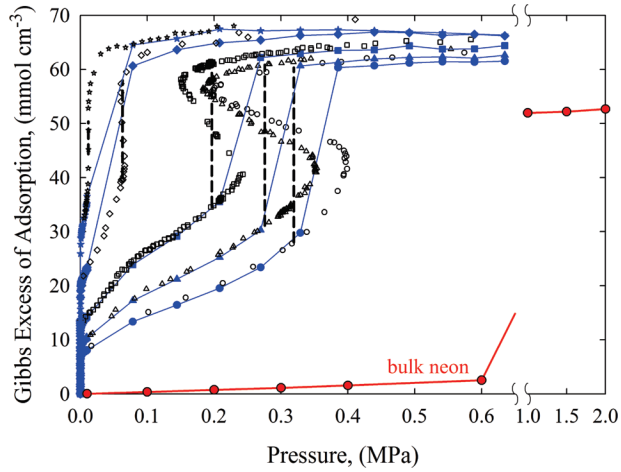

Figure 1. Pore-gauge MC (closed blue symbols and lines) and grand canonical MC isotherms (open black symbols) of classical neon adsorption in atomistic slit-shaped carbon nanopores of different effective pore widths (from left to right): 11.6, 16.6, 26.6, 36.6, and 46.6 Å at 35 K. Dashed vertical lines correspond to first-order vapor−liquid transitions computed from thermodynamic integration, whereas the bulk neon isotherm at 35 K is shown by a solid red line. Note the high compression of classical neon liquidlike adsorbed phases.

III. Results and Discussion

As mentioned by Hofmann and Nielaba,[22] "At low temperatures quantum effects become important, which have been ignored in most of the existing theoretical studies of pore condensate". The equilibrium first-order vapor−liquid phase transition pressures for neon confined in studied graphic slit-shaped carbon nanopores at 35 K computed from classical and quantum simulations are displayed in Figures 1 and 2. To the best our knowledge it is the first calculation of the s-shaped van der Waals isotherms for realistic quantum fluid confined in nanopores. Note that gauge cell and grand canonical path integral MC predict the same values of Gibbs excess of neon adsorption outside the region of vapor−liquid coexistence, as is presented in Figures 1 and 2. As shown by Neimark et al.[38,51−54] and others,[6,28,50] in the homogeneous vapor and liquid phase, the size of a gauge cell plays no role because small fluctuations characteristic of the homogeneous phase are not affected by the finite size of the gauge cell. However, some long-wavelength fluctuations characteristic of the fluid close to the phase transition are restricted by the finite size of the gauge cell. That is why metastable and unstable states can be easily observed in gauge cell simulations, as shown in Figure 3. The whole phase diagram of confined neon is significantly affected by its zero-point motion. First, we found that for all studied carbon nanopores the first-order vapor−liquid phase transition pressures for both classical and quantum neon are shifted down to lower values compared to those for the bulk neon. This shift of the vapor−liquid phase transition is characteristic for nanopores with attractive walls. When neon atoms are treated as classical or quantum particles, their density at fixed bulk pressure in attractive slit-shaped carbon nanopores is higher in comparison to those in the bulk phase, as shown in Figures 1−4. Regardless of the size of the studied carbon pore, adsorbed neon formed dense solid-like discrete layers at the pore walls (see

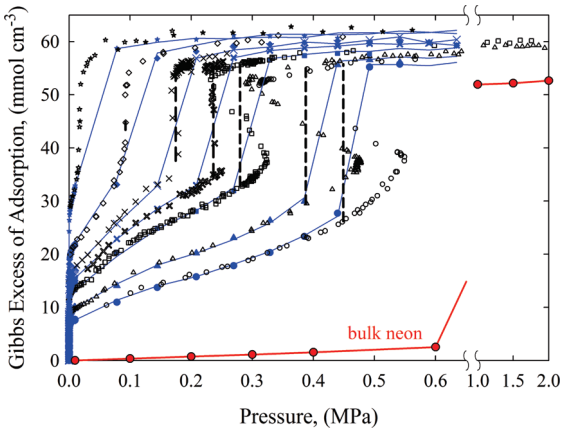

Figure 2. Pore-gauge path integral MC (closed blue symbols and lines) and grand canonical path integral MC isotherms (open black symbols) of quantum neon adsorption in atomistic slit-shaped carbon nanopores of different effective pore widths (from left to right): 11.6, 16.6, 20.6, 23.6, 26.6, 36.6, and 46.6 Å at 35 K. Dashed vertical lines correspond to first-order vapor−liquid transitions computed from thermodynamic integration, whereas the bulk neon isotherm at 35 K is shown by a solid red line. Note the high compression of quantum neon liquidlike adsorbed phases and the regular shift of continuous van der Waals s-shaped isotherms to higher values of pressure in comparison to the classical ones (see Figure 1).

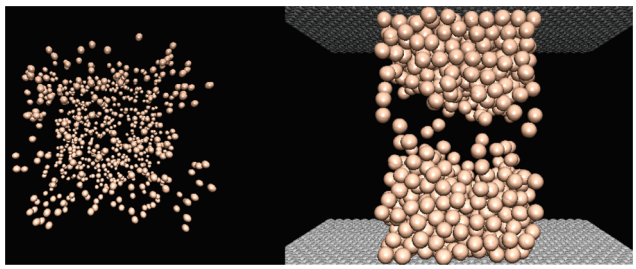

Figure 3. Stabilization of liquid bridge composed of neon paths in a slit-shaped carbon nanopore of effective pore width 46.6 Å at 35 K (left panel) by a finite size gauge cell (right panel). The external bulk pressure of neon is 0.502 MPa, whereas the density of adsorbed neon is 40.78 mmol cm^{-3}.

Figure 4). As a result, vapor−liquid phase transitions are altered in carbon nanopores. However, the most interesting observation is shifting of continuous van der Waals s-shaped isotherms computed from classical simulations down to the lower values of pressures in comparison to those from quantum simulations, as shown in Figures 5 and 6. This systematic underestimation of transition pressures as well as spinodals in classical simulations are caused by neglecting the zero-point motion of adsorbed neon at 35 K. Quantum fluctuations destabilize liquidlike arrangement of adsorbed and compressed neon atoms. That is why, regardless of the size of the slit-shaped carbon pore, classical neon fluid condenses at lower pressures (see phase diagram shown in Figure 6). Interestingly, we found that for all studied slit-shaped carbon nanopores equilibrium vapor−liquid transition pressures computed from quantum simulations are underestimated in classical simulations by ≈30%. As an example, for the widest studied slit-shaped carbon nanopore of H_{eff} = 46.6 Å, the shift of the equilibrium first-order vapor−liquid transition pressure is 29%. Similarly, for the lowest studied slit-shaped carbon nanopore of H_{eff} = 16.6 Å, this shift is around 32%. The size of s-shaped van der Walls isotherms computed from both classical and quantum simulations are reduced with decreasing of the slit-shaped carbon pore size. Above the capillary critical pressure (see phase diagrams displayed in Figure 6), Gibbs excess isotherms are a monotonic function of

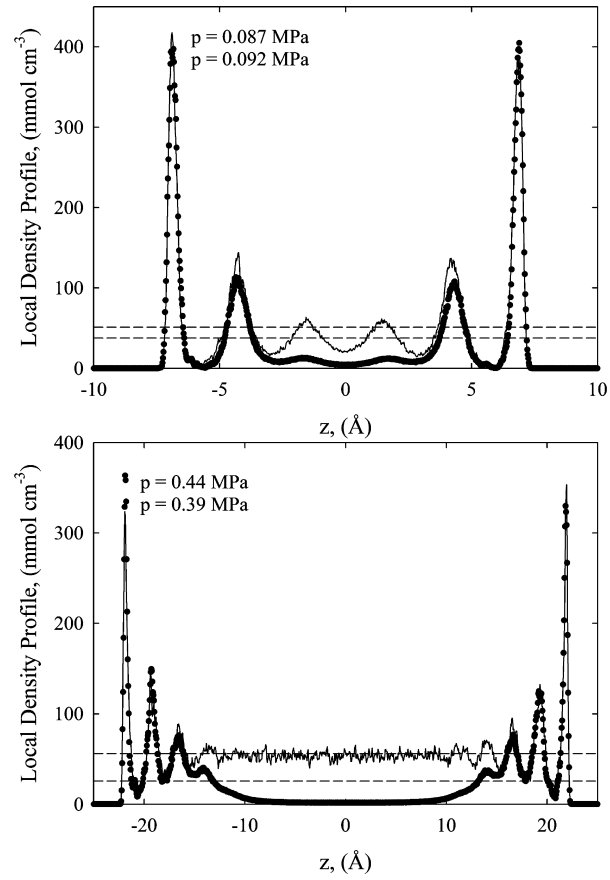

Figure 4. Local centroid−centroid density profiles of quantum neon adsorbed in atomistic slit-shaped carbon nanopores of effective pore widths 11.6 (top panel) and 46.6 Å (bottom panel). Note that for both studied carbon nanopores, adsorbed quantum neon forms solid-like discrete layers at the pore walls before (black circles) and after (solid lines) capillary condensation. Moreover, the middle parts of both studied carbon nanopores are filled by liquidlike neon at 35 K (dashed lines corresponding to bulk densities of neon at selected pressures displayed in the plots).

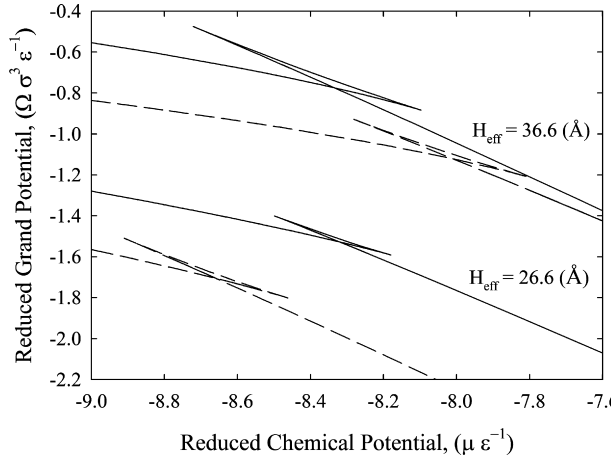

Figure 5. Classical (dashed lines) and quantum (solid lines) neon isotherms of the grand potential at 35 K and two selected sizes of atomistic slit-shaped carbon nanopores: 26.6 and 36.6 Å. Note the shifting of the vapor−liquid phase transition pressures as well as spinodals due to quantum fluctuations of adsorbed and compressed neon atoms.

the external pressure and it is no longer possible to distinguish between vaporlike and liquidlike phases (i.e., confined fluid is supercritical[56]). Clearly, quantum fluctuations shift a capillary critical pressure to higher values, as shown in Figure 6.

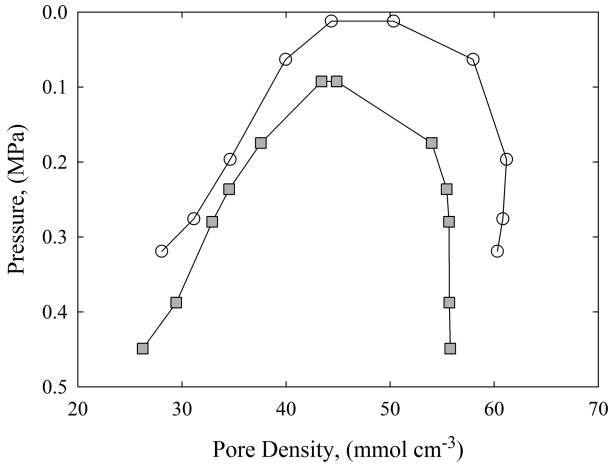

Figure 6. Phase diagram of classical (open circles) and quantum neon (closed squares) adsorbed and compressed in atomistic slit-shaped carbon nanopores at 35 K.

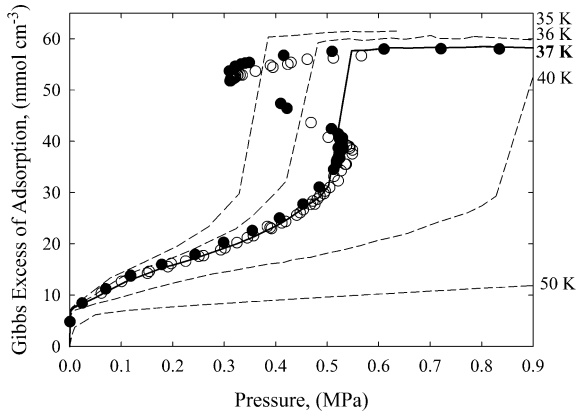

Figure 7. Reproduction of quantum neon adsorption (open circles: gauge cell path integral MC simulations) in atomistic slit-shaped carbon nanopores of effective pore width 46.6 Å at 35 K by classical simulations of neon adsorption at higher effective temperatures (bold solid and dashed lines): 35, 36, 37, 40, and 50 K. Note that the continuous van der Waals s-shaped isotherm computed from quantum neon simulations at 35 K was successfully reproduced by classical simulations of neon adsorption at 37 K (bold solid line, grand canonical MC; closed circles, gauge cell MC).

Delocalized neon atoms excluded more volume in adsorbed phase than classical neon particles. Thus, the maximum densities of adsorbed and compressed delocalized neon atoms are lower than its classical counterpart (see Figures 1 and 2). Following the Heisenberg uncertainty principle, compression of quantum particles (i.e., localization in space) increases their kinetic energy (i.e., delocalization in momentum space). Taking this into account Ceperley[57] and others[44] treated the quantum liquid as a classical one at higher effective temperature. Indeed, our simulation results confirmed this statement. By heating classical neon up to 37 K, we are able to reproduce adsorption isotherms of neon computed from path integral simulations at 35 K, as displayed in Figures 7 and 8. Note that the entire s-shaped van der Waals isotherm of quantum neon adsorbed in slit-shaped carbon nanopore of $H_{\text{eff}} = 46.6$ Å at 35 K is successfully reproduced by classical simulation at 37 K (see Figure 7). To explain our simulations results, we computed the variation of the centroid potential of mean force between neon paths adsorbed in an atomistic slit-shaped carbon nanopore of effective pore width 46.6 Å at 35 K. It is clearly shown that quantum fluctuations soften the intermolecular force between two neon atoms in comparison to their classical counterpart (see Figure

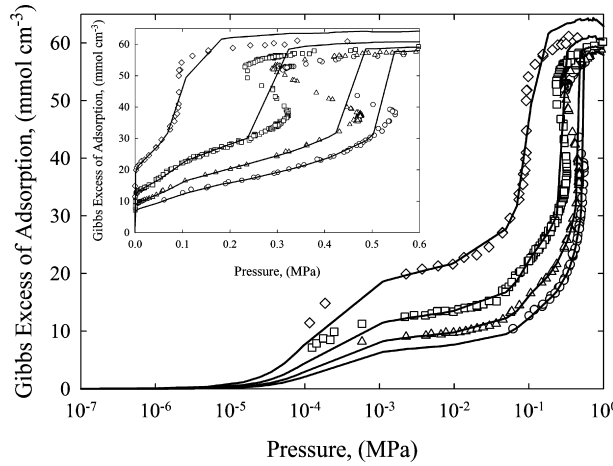

Figure 8. Reproduction of continuous van der Waals s-shaped isotherms computed from quantum simulations of neon adsorption (open symbols: gauge cell path integral MC) in studied slit-shaped carbon nanopores at 35 K by classical simulations of neon adsorption at 37 K. Note that entire adsorption isotherms computed from quantum neon simulations at 35 K were successfully reproduced by classical simulations of neon adsorption at 37 K (bold solid lines: grand canonical MC).

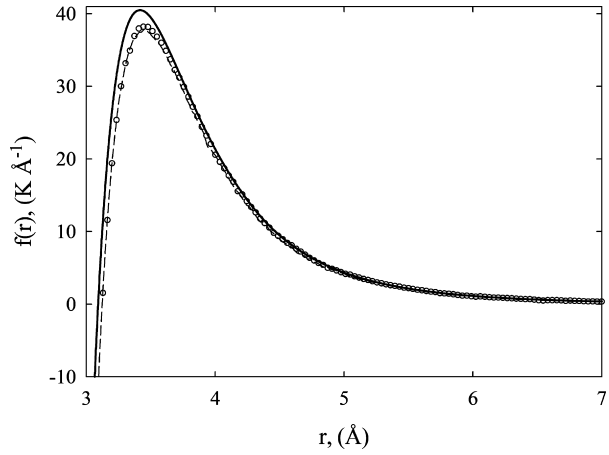

Figure 9. Variation of the centroid potential of mean force between neon paths adsorbed in an atomistic slit-shaped carbon nanopore of effective pore width 46.6 Å at 35 K. The dashed line and open circles correspond to the density of adsorbed neon of 56 and 18 mmol cm^{-3}, respectively. For comparison, the variation of classical force computed from the HFD-B[45] interaction potential is displayed by the solid line. Note that quantum fluctuations lower the attraction depth of the classical force, whereas the hard core repulsion is only slightly shifted to higher values of intermolecular distances.

9). At the same time, the hard core of the effective force is only slightly shifted to the higher values of intermolecular distances. That is why liquidlike phases of confined quantum neon at 35 K look like classical ones at the higher effective temperature of 37 K. However, we want to point out that such simple rescaling of the entire s-shaped van der Waals isotherms of confined quantum neon by classical simulations at higher effective temperature cannot be assumed a priori for any quantum fluid adsorbed in nanoporous material. We speculate that the presented simple picture of confined quantum fluid is restricted by the following ratio: λ/H, where λ is the length of the quantum fluctuations (i.e., the de Broglie wavelength) and H denotes the pore dimension. To support this hypothesis, further research is needed.

Summing up, we show that inclusion of quantum fluctuations is essential for accurate determination of the phase diagram of

quantum fluids confined in nanopores at cryogenic operating conditions. Both classical and quantum phase diagrams of neon adsorbed in slit-shaped carbon nanopores are shifted to lower values of pressures in comparison to those for bulk neon at 35 K. Continuous van der Walls s-shaped isotherms computed from quantum and classical simulations indicate that classical neon fluid condensate at lower values of bulk pressures. Interestingly, we found that adsorption isotherms of neon at 35 K computed from path integral simulations are correctly reproduced by classical simulations at higher effective temperature of 37 K. We explained this observation by taking into account the argument due to Ceperley el al.[57] (i.e., quantum fluid can be treated as classical one at higher effective temperature). However, generalization of this simple rule for other quantum fluids adsorbed in different host nanomaterials and different operating conditions need more theoretical studies.

IV. Conclusions

We present the study of first-order vapor−liquid phase transition of classical and quantum neon confined in atomistic carbon nanopores at 35 K. To the best our knowledge it is the first path integral calculations of continuous van der Waals s-shaped isotherms of a realistic quantum fluid in host nanomaterial. We show that both classical and quantum neon condense at lower pressures than bulk neon because the additional solid−fluid interactions with pore walls accelerate vapor−liquid phase transition. However, the key finding is a regular shifting of continuous van der Waals s-shaped isotherms computed from quantum simulations to higher pressures in comparison to classical ones. Quantum fluctuations destabilize the liquidlike phase of adsorbed and compressed neon as well as increasing its effective volume in the adsorbed phase. As a result, classical simulations overestimate the density of the adsorbed and compressed neon in studied host nanomaterials. Interestingly, we found that adsorption isotherms of neon at 35 K computed from path integral simulations are correctly reproduced by classical simulations at a higher effective temperature of 37 K. Thus, we conclude that neon confined in carbonaceous nanopores at 35 K looks like its classical counterpart at 37 K. Our simulation results clearly show the importance of zero-point motion of light particles adsorbed and compressed in nanopores at cryogenic operating conditions.

Acknowledgment. P.K. gratefully acknowledges Prof. Alina Ciach (Polish Academy of Sciences, Warsaw, Poland) for fruitful correspondences and suggestions on the content of the current paper. P.K. also acknowledges the Royal Melbourne Institute of Technology for a postdoctoral fellowship (2008−2010). P.G. and A.P.T. acknowledge the use of the computer cluster at the Poznan Supercomputing and Networking Centre as well as the Information and Communication Technology Centre of Nicolaus Copernicus University (Torun, Poland).

References and Notes

(1) Kerry, F. G. *Industrial gas handbook: gas separation and purification*; CRC Press: Boca Raton, FL, 2007.
(2) Flynn, T. M. *Cryogenic engineering*; Marcel Dekker: New York, 2005.
(3) Ivanchenko, Y. M.; Lisyansky, A. A. *Physics of critical fluctuations*; Springer-Verlag: New York, 1995.
(4) Kowalczyk, P.; Holyst, R.; Terrones, M.; Terrones, H. *Phys. Chem. Chem. Phys.* **2007**, *9*, 1786.
(5) Jee, S. E.; Sholl, D. S. *J. Am. Chem. Soc.* **2009**, *131*, 7896.
(6) Kowalczyk, P.; Ciach, A.; Neimark, A. V. *Langmuir* **2008**, *24*, 6603.
(7) Brennan, J. K.; Thomson, K. T.; Gubbins, K. E. *Langmuir* **2002**, *18*, 5438.
(8) Tanaka, H.; Kanoh, H.; Yudasaka, M.; Iijima, S.; Kaneko, K. *J. Am. Chem. Soc.* **2005**, *127*, 7511.
(9) Wang, Q.; Challa, S. R.; Sholl, D.; Johnson, J. K. *Phys. Rev. Lett.* **1999**, *82*, 956.
(10) Dubbeldam, D.; Calero, S.; Maesen, T. L. M.; Smit, B. *Angew. Chem., Int. Ed.* **2003**, *42*, 3624.
(11) Kowalczyk, P.; Solarz, L.; Do, D. D.; Samborski, A.; MacElroy, J. M. D. *Langmuir* **2006**, *22*, 9035.
(12) Terzyk, A. P.; Furmaniak, S.; Harris, P. J. F.; Gauden, P. A.; Wloch, J.; Kowalczyk, P.; Rychlicki, G. *Phys. Chem. Chem. Phys.* **2007**, *9*, 5919.
(13) Bhattacharya, S.; Gubbins, K. E. *Langmuir* **2006**, *22*, 7726.
(14) Nicholson, D.; Parsonage, N. G. *Computer Simulation and the Statistical Mechanics of Adsorption*; Academic Press: London, 1982.
(15) Kaneko, K.; Ishii, C.; Ruike, M.; Kuwabara, H. *Carbon* **1992**, *30*, 1075.
(16) Tanaka, H.; El-Merraoui, M.; Steele, W. A.; Kaneko, K. *Chem. Phys. Lett.* **2002**, *352*, 334.
(17) Kowalczyk, P.; Brualla, L.; Zywocinski, A.; Bhatia, S. K. *J. Phys. Chem. C* **2007**, *111*, 5250.
(18) Ravikovitch, P. I.; Vishnyakov, A.; Russo, R.; Neimark, A. V. *Langmuir* **2000**, *16*, 2311.
(19) Tunca, C.; Ford, D. M. *J. Chem. Phys.* **2004**, *120*, 10763.
(20) Kowalczyk, P.; Gauden, P. A.; Terzyk, A. P.; Furmaniak, S. *J. Phys.: Condens. Matter* **2009**, *21*, 144210.
(21) Kowalczyk, P.; Gauden, P. A.; Terzyk, A. P. *J. Phys. Chem. C* **2008**, *112*, 8275.
(22) Hoffmann, J.; Nielaba, P. *Phys Rev E* **2003**, *67*, 036115.
(23) Garberoglio, G. *J. Chem. Phys.* **2008**, *128*, 134109.
(24) Challa, S. R.; Sholl, D.; Johnson, J. K. *Phys. Rev. B* **2001**, *63*, 245419.
(25) Tanaka, H.; Noguchi, D.; Yuzawa, A.; Kodaira, T.; Kanoh, H.; Kaneko, K. *J. Low. Temp. Phys.* **2009**, *157*, 352.
(26) Chandler, D. In *Theory of Quantum Processes in Liquids*; Hansen, J. P., Levesque, D., Zinn-Justin, J., Eds.; Elsevier: Amsterdam, 1991.
(27) Kierlik, E.; Monson, P. A.; Rosinberg, M. L.; Sarkisov, L.; Tarjus, G. *Phys. Rev. Lett.* **2001**, *87*, 055701.
(28) Puibasset, J.; Kierlik, E.; Tarjus, G. *J. Chem. Phys.* **2009**, *131*, 124123.
(29) Kierlik, K.; Puibasset, J.; Tarjus, G. *J. Phys.: Condens. Matter* **2009**, *21*, 155102.
(30) Neimark, V.; Ravikovitch, P. I.; Vishnyakov, A. *Phys. Rev. E* **2002**, *65*, 031505.
(31) Puibasset, J. *J. Phys. Chem. B* **2005**, *109*, 4700.
(32) Monson, P. A. *J. Chem. Phys.* **2008**, *128*, 084701.
(33) Gibbson, R. M. *J. Phys. Chem.* **1968**, *72*, 2567.
(34) Guggenheim, E. A. *J. Chem. Phys.* **1945**, *13*, 253.
(35) Wang, Q.; Johnson, J. K.; Broughton, J. Q. *J. Chem. Phys.* **1997**, *107*, 5108.
(36) Wang, Q.; Johnson, J. K. *Fluid Phase Equilib.* **1997**, *132*, 93.
(37) Kowalczyk, P.; Gauden, P. A.; Terzyk, A. P.; Bhatia, S. K. *Langmuir* **2007**, *23*, 3666.
(38) Neimark, A. V.; Vishnyakov, A. *Phys. Rev. E* **2000**, *62*, 4611.
(39) Feynman, R. P.; Hibbs, A. *Quantum Mechanics and Path Integrals*; McGraw- Hill: New York, 1965.
(40) Feynman, R. P. *Statistical Mechanics*; Benjamin: New York, 1972.
(41) Ceperley, D. M. *Rev. Mod. Phys.* **1995**, *67*, 279.
(42) Ceperley, D. M. *Rev. Mod. Phys.* **1999**, *71*, S438.
(43) Sesé, L. M. *Mol. Phys.* **1994**, *81*, 1297.
(44) Kowalczyk, P.; Brualla, L.; Gauden, P. A.; Terzyk, A. P. *Phys. Chem. Chem. Phys.* **2009**, *11*, 9182.
(45) Aziz, R. A.; Slaman, M. *J. Chem. Phys.* **1989**, *130*, 187.
(46) Allen, M. P.; Tildesley, D. J. *Computer Simulation of Liquids*; Clarendon: Oxford, U.K., 1987.
(47) Frenkel, D.; Smit, B. *Understanding Molecular Simulation From Algorithms To Applications*; Academic Press: London, 1996.
(48) Do, D. D. *Adsorption analysis: equilibria and kinetics*; Imperial College Press: London, 1998.
(49) Singer, K.; Smith, W. *Mol. Phys.* **1988**, *64*, 1215.
(50) Kowalczyk, P.; Holyst, R.; Tanaka, H.; Kaneko, K. *J. Phys Chem. B* **2005**, *109*, 14659.
(51) Neimark, A. V.; Vishnyakov, A. *J. Phys. Chem. B* **2005**, *109*, 5962.
(52) Neimark, A. V.; Vishnyakov, A. *J. Chem. Phys.* **2005**, *122*, 054707.
(53) Neimark, A. V.; Vishnyakov, A. *J. Chem. Phys.* **2005**, *122*, 234108.
(54) Vishnyakov, A.; Neimark, A. V. *J. Chem. Phys.* **2003**, *119*, 9755.
(55) Widom, B. *J. Chem. Phys.* **1963**, *39*, 2808.
(56) Evans, R.; Marconi, M. B.; Tarazona, P. *J. Chem. Phys.* **1986**, *84*, 2376.
(57) Ceperley, C. M.; Pollock, E. L. *Can. J. Phys.* **1987**, *65*, 1416.

JP911189J